Facile Synthesis and High Performance of a New Carbazole-Based Hole-Transporting Material for Hybrid Perovskite Solar Cells — Source link ⧉

Hong Wang, Arif D. Sheikh, Quanyou Feng, Quanyou Feng ...+11 more authors

Institutions: Nanjing University of Posts and Telecommunications, Fudan University

Topics: Perovskite solar cell, Hybrid solar cell, Perovskite (structure) and Energy conversion efficiency

Related papers:

- Organometal Halide Perovskites as Visible-Light Sensitizers for Photovoltaic Cells

- Carbazole-Based Hole-Transport Materials for Efficient Solid-State Dye-Sensitized Solar Cells and Perovskite Solar Cells

- Novel Carbazole-Based Hole-Transporting Materials with Star-Shaped Chemical Structures for Perovskite-Sensitized Solar Cells

- Lead Iodide Perovskite Sensitized All-Solid-State Submicron Thin Film Mesoscopic Solar Cell with Efficiency Exceeding 9%

- Triazatruxene-Based Hole Transporting Materials for Highly Efficient Perovskite Solar Cells

Share this paper: 🄕 🐦 in ✉

View more about this paper here: https://typeset.io/papers/facile-synthesis-and-high-performance-of-a-new-carbazole-gtrmvznh8b

Facile Synthesis and High performance of a New Carbazole-Based Hole Transporting Material for Hybrid Perovskite Solar Cells

Hong Wang, Arif D. Sheikh, Quanyou Feng, Feng Li, Yin Chen, Weili Yu, Erkki Alarousu, Chun Ma, Md Azimul Haque, Dong Shi, Zhong-Sheng Wang, Omar F. Mohammed, Osman M. Bakr, and Tom Wu

Just Accepted

Facile Synthesis and High performance of a New Carbazole-Based Hole Transporting Material for Hybrid Perovskite Solar Cells

Hong Wang* [a,⊥], Arif D. Sheikh[a,⊥], Quanyou Feng[b,c], Feng Li[a], Yin Chen[a], Weili Yu[a],

Erkki Alarousu[d], Chun Ma[a], Md Azimul Haque[a], Dong Shi[a], Zhong-Sheng Wang[b],

Omar F. Mohammed[d], Osman M. Bakr[a], Tom Wu*[a]

[a] Materials Science and Engineering, King Abdullah University of Science and Technology (KAUST), Thuwal 23955, Saudi Arabia

[b] Department of Chemistry, Lab of Advanced Materials, Collaborative Innovation Center of Chemistry for Energy Materials, Fudan University, Songhu Road 2205, 200438 Shanghai, P. R. China

[c] Center for Molecular Systems and Organic Devices (CMSOD), Key Laboratory for Organic Electronics & Information Displays (KLOEID) and Institute of Advanced Materials (IAM), National Jiangsu Synergetic Innovation Center for Advanced Materials (SICAM), Nanjing University of Posts & Telecommunications, 9 Wenyuan Road, Nanjing 210023, P. R. China

[d] Solar and Photovoltaics Engineering Research Center, Division of Physical Sciences and Engineering, King Abdullah University of Science and Technology (KAUST), Thuwal 23955, Saudi Arabia

KEYWORDS: perovskite solar cell, carbazole, hole transporting material, hole mobility

1

ABSTRACT: Perovskite solar cells are very promising for practical applications owing to their rapidly rising power conversion efficiency and low cost of solution-based processing. 2,2',7,7'-tetrakis-(N,N-di-p-methoxyphenylamine) 9,9'-spirobifluorene (Spiro-OMeTAD) is most widely used as hole transporting material (HTM) in perovskite solar cells. However, the tedious synthesis and high cost of Spiro-OMeTAD inhibit its commercial-scale application in the photovoltaic industry. In this article, we report a carbazole-based compound (**R01**) as a new HTM in efficient perovskite solar cells. **R01** is synthesized via a facile route consisting of only two steps from inexpensive commercially available materials. Furthermore, **R01** exhibits higher hole mobility and conductivity than the state-of-the-art Spiro-OMeTAD. Perovskite solar cells fabricated with **R01** produce a power conversion efficiency of 12.03%, comparable to that obtained in devices using Spiro-OMeTAD in this study. Our findings underscore **R01** as a highly promising HTM with high performance, and its facile synthesis and low cost may facilitate the large-scale applications of perovskite solar cells.

2

Photovoltaic technologies hold promise for meeting the escalating worldwide demands of renewable energies. Since 2009, perovskite solar cells have attracted considerable attention due to their high efficiency of converting solar energy to electricity with solution processing and low cost.[1-5] Typically, the perovskite solar cell is composed of a perovskite/mesoporous TiO_2 layer sandwiched between layers of electron-transporting (hole-blocking) TiO_2 and a hole transporting material (HTM). Absorption of sunlight by the perovskite generates electron-hole pairs, which then transport through TiO_2 and HTM, before being collected by the electrodes. Organic HTMs are promising candidates in high-performance perovskite solar cells due to their versatile molecular structures and excellent photoelectrical properties.[6-11] Among them, 2,2',7,7'-tetrakis-(N,N-di-p-methoxyphenylamine) 9,9'-spirobifluorene (Spiro-OMeTAD) is most widely used to achieve high efficiency in perovskite solar cells.[3,4] For example, a very high efficiency of 19.3% was recently achieved for perovskite solar cells with Spiro-OMeTAD as the HTM.[4] However, the onerous synthesis and exorbitant cost of Spiro-OMeTAD inhibit its up-scale application in photovoltaic industry.[12] As alternatives, various inorganic materials such as CuI[13] and CuSCN[14-15] have been used as HTMs in perovskite solar cells. But the inorganic semiconductors usually suffer from low conductivity, and the perovskite solar cells using such HTMs exhibit low efficiencies. Therefore, developing new HTMs with high performance yet low cost is of great importance from the practical point of view.

3

Carbazole-based HTMs have been proven to be promising materials in both organic light emitting diodes and solar cells, owing to their excellent charge-transport and photoelectric properties.[16-18] It is known that the highest occupied molecular orbital (HOMO) level of carbazole-based donor is slightly lower than that of triphenyl amine based donor.[19-20] In general, the open-circuit voltage V_{oc} of perovskite solar cells is determined by the difference between the quasi-Fermi level of the electrons in the TiO_2 and that of the holes in the HTM.[21] Therefore, a higher V_{oc} is anticipated for the perovskite solar cells with carbazole-based HTM compared to the ones based on Spiro-OMeDA because the donor of the latter is triphenyl amine derivate.[22] Carbazole-based compounds caught the attention of researchers as novel HTMs,[16] but the synthesis of such materials often involves multiple steps, including protection and deprotection. Therefore, in the race of novel HTMs for perovskite solar cells, the design and synthesis of novel organic compounds with simplified synthetic routes but excellent hole-transport properties remains highly desired.

Herein, we report a novel high-performance HTM, **R01**, with very simple molecular structure, which was synthesized via a facile route with low cost and high yield. The structures of **R01** and Spiro-OMeTAD are shown in Scheme 1. **R01** is carbazole-based and bridged by 3,4-ethylenedioxythiophene. Its structure is much simpler than not only Spiro-OMeTAD but also other organic HTMs reported to date (Table S1). The much smaller size of the **R01** allows a deeper penetration into the mesoporous TiO_2, which facilitates the hole extraction, thus improving device

4

performance. In this work, the perovskite solar cells device using **R01** as HTM shows

efficiency η of 12.03% and V_{oc} of 0.98 V under the irradiation of simulated AM1.5G

solar light. Our findings make **R01** a very promising alternative HTM in perovskite

solar cells, and its facile synthesis may facilitate driving down the fabrication cost of

perovskite-based photovoltaic technology.

R01

Molecular weight: 528.67

Spiro-OMeTAD

Molecular weight: 1225.46
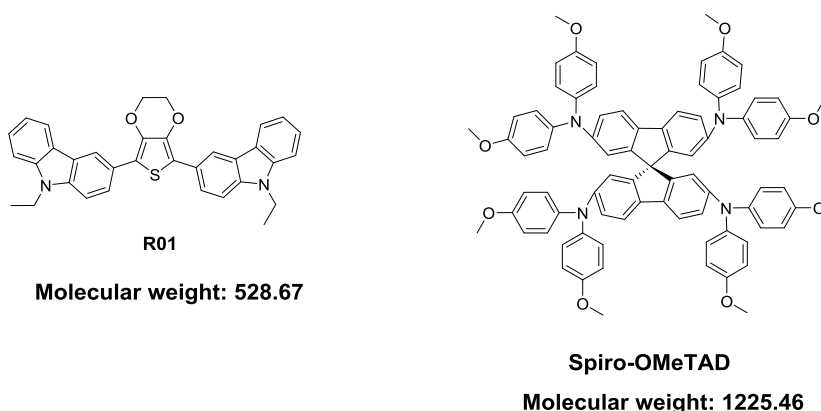
Scheme 1. Molecular structures of the HTM **R01** and Spiro-OMeTAD. The molecular

weights are given in g/mol.

The facile synthesis of **R01** was achieved in only two simple steps with inexpensive

commercial materials, which is much more straightforward than Spiro-OMeTAD.

Briefly, 9-ethyl-3-(4,4,5,5-tetramethyl-1,3,2-dioxaborolan-2-yl)-9H-carbazole was

first synthesized according to the reported method.[23] **R01** as yellow powders (Figure

S1) was then obtained by reacting commercial

5,7-Dibromo-2,3-dihydrothieno[3,4-b][1,4]dioxine with

9-ethyl-3-(4,4,5,5-tetramethyl-1,3,2-dioxaborolan-2-yl)-9H-carbazole through

palladium-catalyzed Suzuki-Miyaura cross-coupling reaction (Scheme S1). The facile

5

synthesis has a high yield of 73%. More synthesis details can be found in the

experimental section.
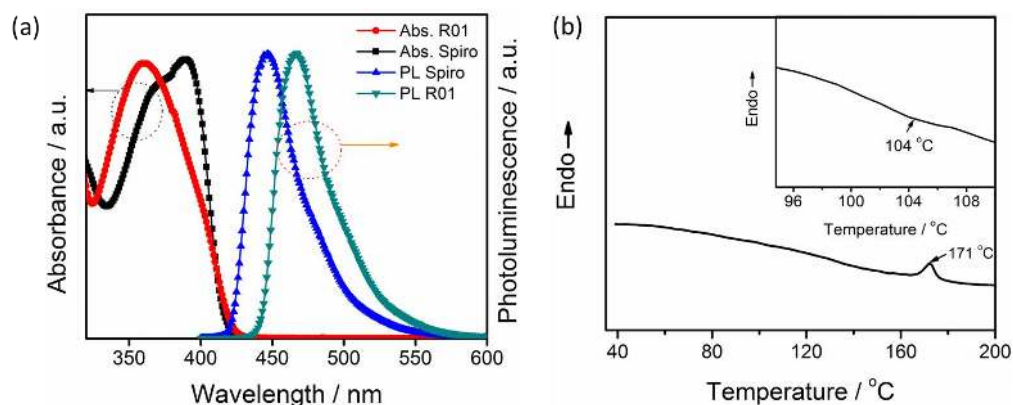
Figure 1. (a) Absorption and emission spectra of **R01** and Spiro-OMeTAD. (b) DSC curve of

R01 with the melting temperature being marked by an arrow. Inset shows the region around

the glass transition temperature.

The absorption and photoluminescence spectra of **R01** and Spiro-OMeTAD are

shown in Figure 1a, and the corresponding properties are listed in Table 1. The

maximum absorption peak of **R01** appears at 360 nm, which is a blue shift of 27 nm

relative to that of Spiro-OMeTAD. Moreover, the fluorescence emission peaks of **R01**

and Spiro-OMeTAD are located at 467 and 446 nm, respectively, i.e., **R01** exhibits a

red shift of 21 nm relative to Spiro-OMeTAD. Correspondingly, the Stokes shifts of

R01 and Spiro-OMeTAD as determined by the equation $\Delta\lambda = \lambda_{em} - \lambda_{abs}$ are 107 nm

and 59 nm, respectively. Compared to Spiro-OMeTAD, the much larger Stokes shift

of **R01** implies that **R01** can undergo much more geometrical changes upon

excitation.[11] Therefore, the larger Stokes shift in combination with the smaller size of

R01 permits better filling into the porous TiO_2 films, which is beneficial for

6

enhancing the hole-extracting efficiency in solar cells. The thermal stability of **R01** was examined using the thermal gravimetric analysis (TGA). The TGA data indicate that R01 is quite stable and its thermal degradation starts at 388 °C (Figure S2). Differential scanning calorimetry (DSC) curve (Figure 1b) shows that the glass transition temperature (T_g) and the melting point (T_m) of R01 are 104 °C and 171 °C, respectively, which are lower than those of Spiro-OMeTAD (T_g=125 °C and T_m=248 °C).[24]

Tabl 1. Optical and electronic properties of **R01** and Spiro-OMeTAD.

HTM	λ_{abs}/nm	λ_{em}/nm	E_g[a] /eV	HOMO/eV	LUMO/eV[b]
R01	360	467	2.88	-5.30	-2.42
Spiro-OMTAD	387	446	2.91	-5.24	-2.33

[a] Optical band gap (E_g) obtained from the onset value of absorption; [b] LUMO calculated by LUMO=HOMO+E_g.

To determine and compare the oxidation potential of **R01** and Spiro-OMeTAD, cyclic voltammetry (CV) measurements were carried out with HTMs in a solution of tetrabutylammonium hexafluorophosphate (0.1 M) in dichloromethane. The scan rate is 50 mV s^{-1}, and the data are shown in Figure 2a. The HOMO levels of **R01** and Spiro-OMeTAD, taken from the first oxidation potential, were calculated as 5.30 eV and 5.24 eV, respectively (Table 1). As expected, the HOMO level of the carbazole-based **R01** is lower than that of the triphenyl-amine-based Spiro-OMeTAD

7

by about 60 mV. Therefore, we anticipate a higher V_{oc} value for the **R01**-based perovskite solar cells than the ones with Spiro-OMeTAD.

It is well known that chemical p-doping is a powerful tool to lower the HOMO level and to improve the charge-transport properties of organic semiconductings.[25] However, the defects associated with the p-dopants could limit the performance of perovskite solar cells.[26] Therefore, the optimal p-dopant should satisfy the following criteria: the position of oxidation potential of the dopant with respect to the energy levels of host should give enough driving force to extract the holes; the p-dopant should have good solubility in the HTM. In this work, we chose tris[2-(1H-pyrazol-1-yl)pyrimidine]cobalt(III) tris[bis(trifluoromethylsulfonyl)imide, MY11[26] as the dopant because of its relative high oxidation potential and good solubility compared to the commonly used FK102. The structure of MY11 is shown in Figure S3, and its synthetic is detailed in the Supporting Information.

Figure 2b shows the UV/vis absorption spectra of the **R01** solutions upon the gradual addition of MY11. It can be clearly seen that the oxidized **R01** species progressively increase in the light absorption in the visible range of 425-650 nm. After the effective chemical doping, the enhancements of both V_{oc} and fill factor (FF) of solar cells with **R01** are expected because V_{oc} is approximately determined by the difference between the Fermi level of the TiO_2 and the HOMO level of **R01,** while the FF is related to the charge-transport properties of **R01**.[27]

8

Conductivity measurements (Figure 2c and Table 2) indicate that the conductivities of pristine **R01** and Spiro-OMeTAD are 9.39×10^{-5} and 7.72×10^{-5} S•cm^{-1}, respectively. It should be mentioned that the conductivity of **R01** is notably higher than that of Spiro-OMeTAD. Moreover, the conductivity of **R01** gradually increases with increasing MY11 content as a result of the effective p-doping. When the doping level of MY11 reaches 12 mol%, which is the solubility limit, the conductivity increases by two orders of magnitude and reaches 9.24×10^{-3} S•cm^{-1}.
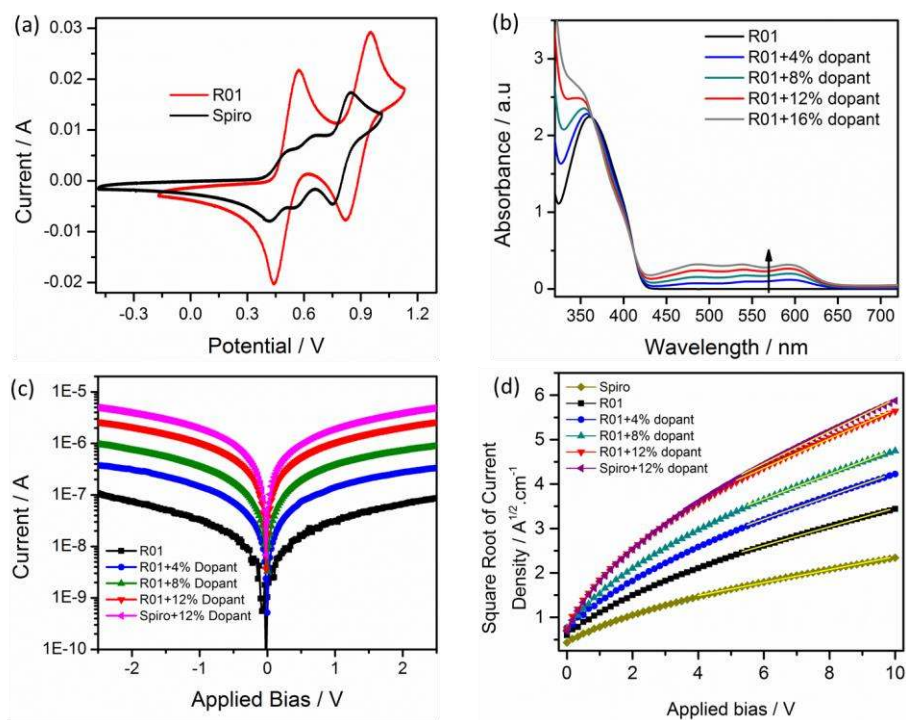

Figure 2. (a) CV curves of R01 and Spiro-OMeTAD. (b) Absorption spectra of **R01** with different doping concentrations in chlorobenzene. (c) Current-voltage characteristics of pristine and doped HTM films. (d) Current density-voltage characteristics of hole-conducting layers and the straight lines represent fittings to the SCLC mechanism.

9

We further studied the effect of doping on the hole mobility μ of **R01** by measuring the space-charge-limited current (SCLC).[28] The current density vs. voltage data in Figure 2d were fitted to the equation,

$$J = \frac{9}{8} \varepsilon_0 \varepsilon \mu \frac{V^2}{d^3} \qquad (1)$$

where ε is the dielectric constant and d is the film thickness. The value of mobility obtained here (8.19×10^{-5} $cm^2 \cdot V^{-1} \cdot s^{-1}$) for Spiro-OMeTAD is close to the ones reported in literature.[16, 26] Importantly, the hole mobility of **R01** (2.05×10^{-4} $cm^2 \cdot V^{-1} \cdot s^{-1}$) is about three times higher than that of Spiro-OMeTAD, indicating a much faster hole-transport capability. In addition, doping MY11 is very effective to increase the hole mobility of **R01**, and the highest mobility was found to be 4.78×10^{-4} $cm^2 \cdot V^{-1} \cdot s^{-1}$ at the doping level of 12 mol%.

Table 2. Electrical properties and the photovoltaic parameters of perovskite solar cells with different HTMs.

HTMs with different dopant	Conductivity $(S \cdot cm^{-1})$	Hole mobility $(cm^2 \cdot V^{-1} \cdot s^{-1})$	V_{oc} (V)	J_{sc} $(mA \cdot cm^{-2})$	*FF*	*η%*
R01	9.36×10^{-5}	2.05×10^{-4}	0.86	16.7	0.522	7.47
Spiro-OMeTAD	7.72×10^{-5}	8.19×10^{-5}	0.84	16.8	0.542	7.66
R01+4 mol% dopant	2.20×10^{-4}	2.87×10^{-4}	0.91	17.4	0.554	8.78
R01+8 mol% dopant	3.78×10^{-3}	3.54×10^{-4}	0.93	17.6	0.599	9.82
R01+12 mol% dopant	**9.24×10^{-3}**	**4.78×10^{-4}**	**0.98**	**17.9**	**0.687**	**12.03**
Spiro+12 mol% dopant	9.57×10^{-2}	5.02×10^{-4}	0.94	18.0	0.718	12.17

The cross-sectional scanning electron microscope (SEM) image of a typical perovskite solar cell is shown in Figure 3. One-step deposition method was used to

10

prepare the $CH_3NH_3PbI_{3-x}Cl_x$ perovskite/mesoporous TiO_2 layer (640 nm thick)

sandwiched between the compact TiO_2 (40 nm thick) and the **R01** layers (100 nm

thick).[26] An Au layer with the thickness of about 140 nm was evaporated on the top

of **R01** as the cathode. As shown in Figure 4a and Table 2, under the irradiation of

simulated AM1.5G solar light, the device using the pristine **R01** as the hole-

transporting layer exhibits η of 7.47% (V_{oc}=0.86 V, J_{sc}=16.66 mA/cm^{-2}, and

FF=0.522). Importantly, all performance parameters of the **R01**-based devices were

progressively improved with increasing MY11 content. The device based on **R01** with

12 mol% dopant exhibits the highest power conversion efficiency of 12.03%. At the

same time, V_{oc} increases from 0.86 V to 0.98 V, J_{sc} from 16.66 mA/cm^{-2} to 17.87

mA/cm^{-2}, and FF from 0.522 to 0.687. The enhancement of V_{oc} in the devices is a

result of the lowered HOMO level of **R01** after the MY11 doping. The improved

conductivity and hole mobility of the **R01** after doping are responsible for the

increased J_{sc} and FF.

In a control experiment, we fabricated devices using Spiro-OMeTAD as the HTM,

and the obtained maximum η value is 7.66% (V_{oc}=0.84 V, J_{sc}=16.83 mA/cm^{-2}, and

FF=0.542). Thus, the performance of the **R01**-based device is comparable to the

device using the state-of-the-art Spiro-OMeTAD. As expected, V_{oc} of the device with

R01 is slightly higher than that of the Spiro-OMeTAD counterpart, which also holds

true after doping. This improvement of V_{oc} can be attributed to the relatively lower

HOMO level of **R01** than that of Spiro-OMeTAD, consistent with the electrochemical

11

measurement result. Furthermore, as shown in the photocurrent density-voltage (J-V) curves in Figure 4a, the dark current of the **R01**-based devices decreases progressively with increasing MY11 concentration from 0% to 12 mol%, indicating the continuous reduction of charge recombination due to the improved conductivity and hole mobility of **R01** after doping. It is worth noting that the perovskite solar cell based on **R01** with 12 mol% dopant shows a relatively lower dark current and higher onset voltage compared to the device with Spiro-OMeTAD, which is also responsible for the higher V_{oc}.
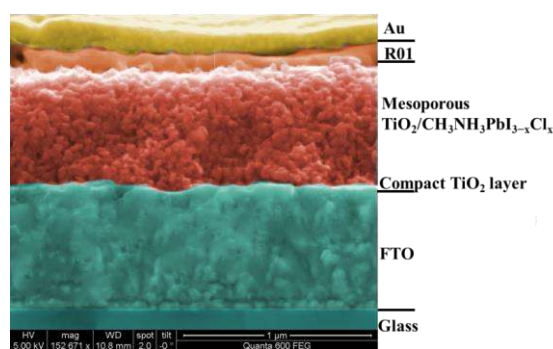
Figure 3. Cross-sectional SEM image of the perovskite solar cell.

It is noteworthy that the maximum η of the **R01**-based devices in this study was achieved with the dopant concentration of 12 mol% which is lower than that of the reported FK102 (15 mol%).[10] This can be explained by the higher oxide potential of MY11 compared to that of FK102. Correspondingly, as shown in Figure 4b, the incident-photon-to-current conversion efficiency (IPCE) spectra of the perovskite solar cells incorporating **R01** exhibit a broad working range from 350 nm to 800 nm,

12

and the maximum IPCE value increases gradually with increasing MY11 concentration, which is in accordance with the tendency of the *J-V* characteristics.

Figure 4. J-V characteristics (a) and the corresponding IPCE spectra (b) of perovskite solar cells with different HTMs.

We used transient absorption spectroscopy to investigate the charge transfer at the perovskite/HTM interface because this technique can provide direct evident on the carrier dynamics including charge transfer a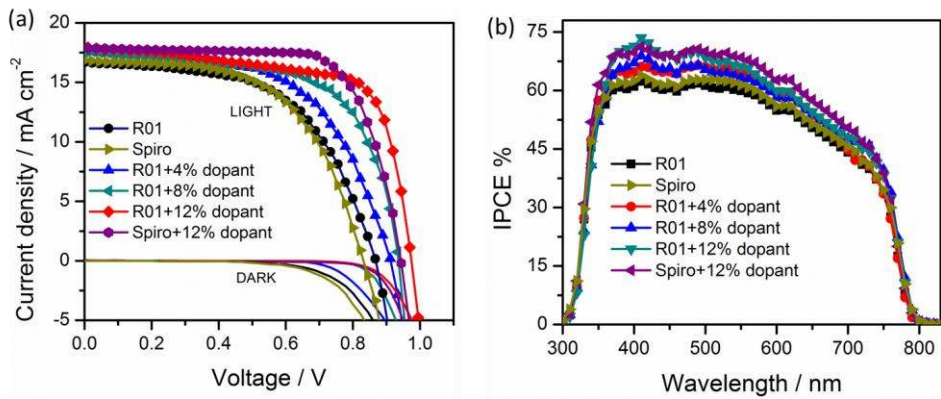nd recombination. As shown in Figure 5a, the negative absorption peak at around 760 nm is a result of the ground-state bleach of perovskite. The carrier dynamics shown in Figure 5b are analyzed by fitting the kinetic data with a two-exponential decay function: $\Delta A = A_1 \exp(-t/\tau_1) + A_2 \exp(-t/\tau_2)$, where A_i and τ_i, i = 1 and 2, are the time-independent coefficients and time constants, respectively. For the perovskite/**R01** bilayer, $\tau_1 = 10.88 \pm 2.60$ ns and $\tau_2 = 40.49 \pm 2.24$ ns were obtained, while in the case of perovskite/Spiro-OMeTAD, the time constants are $\tau_1 = 7.20 \pm 1.97$ ns and $\tau_2 = 40.20 \pm 1.34$ ns. These data reveal that the carrier recombination of the perovskite-**R01** bilayer is comparable to that of the perovskite/Spiro-OMeTAD counterpart. Clearly, the superb properties of

13

R01 such as small size, facile synthesis, large Stocks shift and low HOMO level,

make it highly promising for applications in large-scale production of perovskite solar

cells.
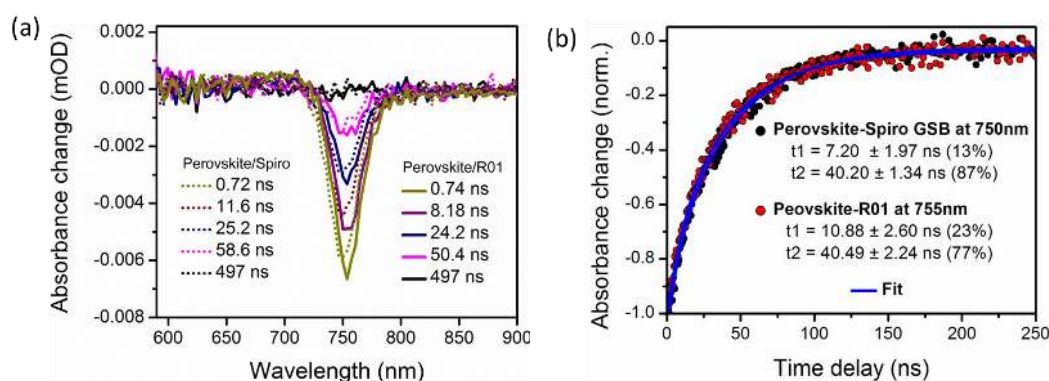
Figure 5. Transient absorption spectra of (a) perovskite/Spiro-OMeTAD and perovskite/R01

films measured after excitation at 480 nm. (b) Normalized kinetic traces for the ground-state

bleach recovery of perovskite-Spiro-OMeTAD and perovskite-R01 bilayers probed at 760 nm

and 755 nm, respectively.

In Table S1, we compare the physical properties and performance of **R01** with other

organic HTMs reported so far in literature. It is clear that the performance of **R01** is

comparable to the best HTMs, while its structure and synthesis are much simpler.

Spiro-OMeTAD remains as the dominant HTM in the research field of perovskite

solar cells with record-high performances, but it may not be the ultimate HTM for

industry-scale production of perovskite solar cells because of its high cost (331.0

EUR per g). Furthermore, we should note that carbazole-based HTMs consistently

exhibit low HOMO levels and high device efficiencies, and this class of organic

14

materials deserve more attention in the search of HTMs with easy synthesis, low cost and high performance for practical applications of perovskite solar cells. We believe that engineering the composition and morphology of perovskite layers as well as their interfaces with charge transporting layers can significantly increase the efficiency of solar cells using such HTMs.

In summary, a novel carbazole-based HTM **R01** with tunable p doping has been successfully designed and synthesized. Because of its relatively small size, structural flexibility and low HOMO level, **R01** showed very good performances as HTM in perovskite solar cells. The highest power conversion efficiency (η = 12.03%) achieved in devices fabricated with **R01** is comparable to that of the control devices with Spiro-OMeTAD (η = 12.17%) fabricated in this study. These results underscore **R01** as a very promising HTM candidate with high performance, and its relatively facile synthesis and low cost will motivate further experimental works and potentially facilitate the large-scale applications of perovskite solar cells.

Experimental Section

Synthesis: The details of materials can be found in Supporting Information. The synthesis of 5,7-Bis(9-ethyl-9H-carbazol-3-yl)-2,3-dihydrothieno[3,4-b][1,4]dioxine, **R01**, is much more succinct than that of Spiro-OMeTAD. 9-ethyl-3-(4,4,5,5-tetramethyl-1,3,2-dioxaborolan-2-yl)-9H-carbazole was synthesized according to the reported methods.[23] **R01** could be obtained through

15

palladium-catalyzed Suzuki-Miyaura cross-coupling reaction (Scheme S1) with a high

yield of 73%. A mixture of

9-ethyl-3-(4,4,5,5-tetramethyl-1,3,2-dioxaborolan-2-yl)-9H-carbazole (1.172 g, 3.65

mmol), 2,5-dibromo-3,4-ethylenedioxythiophene (542 mg, 1.81 mmol), $Pd(PPh_3)_4$

(100 mg, 0.09 mmol), K_2CO_3 (2.76 g, 20 mmol), THF (20 mL), toulene (20 mL) and

H_2O (10 mL) was refluxed for 24 h under N_2. After cooling, water was added and the

reaction mixture was extracted three times with CH_2Cl_2. The combined organic layer

was washed with H_2O and brine, dried over anhydrous Na_2SO_4, and evaporated under

reduced pressure. The crude product was purified by column chromatography

($PE/CH_2Cl_2 = 2/1$) on silica gel to yield the product as a yellow solid. (699 mg, 73%).

1H NMR (400 MHz, DMSO-d_6, ppm): 8.34-8.38 (m, 1H), 8.08-8.17 (m, 3H),

7.82-7.93 (m, 2H), 7.42-7.67 (m, 6H), 7.19-7.27 (m, 2H), 4.49-4.57 (m, 4H), 4.28 (s,

4H), 1.34-1.39 (m, 6H); 13C NMR (100 MHz, DMSO-d_6, ppm): 140.53, 138.87,

138.38, 126.64, 124.29, 122.63, 121.09, 119.57, 117.79, 114.57, 110.06, 109.92,

65.18, 37.63, 14.36. MALDI-TOF-MS (m/z): calcd. For $C_{34}H_{28}N_2O_2S$: 528.2 [M+];

Found: 528.1. Synthesis of tris[2-(1H-pyrazol-1-yl) pyrimidine]cobalt((III) tris

[bis(trifluoromethylsulfonyl)imide can be found in the Supporting Information.

Methylammonium iodide (MAI) was synthesized following a previously reported

procedure[29] To form the non-stoichiometric $CH_3NH_3PbI_{3-x}Cl_x$ precursor solution,

methylammonium iodide and lead (II) chloride (Aldrich, 99%) are dissolved in

anhydrous N,N-dimethylformamide at a 3:1 molar ratio of MAI to $PbCl_2$.

16

Solar Cell Fabrication: Solar cell devices were fabricated on fluorine-doped tin oxide

(FTO) coated glass (Pilkington). First, the FTO was etched with 2 M HCl and zinc

metal powder to define the electrodes. Substrates were then sonicated sequentially in

2% Hellmanex detergent, deionized water, and after drying finally treated with

oxygen plasma. A hole-blocking layer of compact TiO_2 was deposited by spin-coating

(2000 rpm for 60 sec) a mildly acidic solution of titanium isopropoxide in anhydrous

ethanol, and annealed at 500°C for 30 min. Then, 600 nm of mesoporous TiO_2 was

deposited by spin coating a solution of dyesol paste in ethanol with a mass ratio of

1:2.5 at 2000 rpm for 60 sec. This mesoporous layer was sintered at 500 °C for 60

min. To fabricate the perovskite layers, a non-stoichiometric $CH_3NH_3PbI_{3-x}Cl_x$

precursor solution was spin-coated on the mesoporous TiO_2 in a nitrogen-filled glove

box, at 2000 rpm for 45 sec. After spin coating, the films were left to dry at room

temperature in the glove box for 5 minutes followed by annealing on a hotplate in the

glove box at 95°C for 60 minutes. **R01** and Spiro-OMeTAD were each dissolved in

chlorobenzene (100 mg mL^{-1}). tert-butylpyridine (TBP; 15.92 mL) and lithium

bis(trifluoromethylsulfonyl)imide (LiTFSI, 9.68 mL, 520 mg mL^{-1} in acetonitrile)

were added directly to 0.3 mL of the HTM solutions.

Tris[2-(1H-pyrazol-1-yl)pyrimidine]cobalt(III) tris[bis(trifluoromethylsulfonyl)imide,

MY11] was predissolved into acetonitrile and added into the HTM solution with

ratios of 0-12 mol%. The coating process was carried out at 2000 rpm for 30 sec, and

then the devices were stored overnight in the dark under dry air. The humidity level

17

was about 30%. Finally, gold electrodes were deposited by thermal evaporation to complete the fabrication of the solar cells.

Characterizations: ^{1}H and ^{13}C NMR spectra were recorded by using Bruker AVANCE III 400 MHz instruments with tetramethylsilane (TMS) as the internal standard. Mass spectra (MS) and high-resolution MS (HRMS) were performed using a Waters LCT Premier XE spectrometer. The absorption spectra of HTMs in solutions were measured with a Varian Cary 500 spectrophotometer. Extinction spectra were measured on a Varian Cary 5000 UV−vis−NIR spectrophotometer. Differential scanning calorimetry (DSC) data was taken using Shimadzu DSC-60A in a temperature range of 40-200 °C at a heating rate of 5 °C min^{-1}. A field emission scanning electron microscope (FESEM, FEI Quanta 600FEG) was used to acquire cross-section SEM images. Cyclic voltammetry measurements were carried out on a CHI411 electrochemical workstation with HTM in a solution of tetrabutylammonium hexafluorophosphate (0.1 M) in dichloromethane with a scan rate of 50 mV s^{-1}. The Ag/AgCl electrode was used as the reference electrode and platinum wire as the working electrode. Charge transport properties of the HTMs were investigated according to the procedure reported in literature.[25] HTM films were deposited on glass substrates by drop casting in dry air, followed by dark storage overnight. Their transport characteristics were measured with a Keithley 2420 source meter. Helios UV-NIR femtosecond transient absorption spectroscopy was used to measure the samples in this study. The experimental setup was detailed elsewhere[30]. The solar

18

cell performance was measured using a solar simulator (Newport, Oriel Class A, 91195A) at 100 mA cm^{-2} illumination (AM 1.5G), which was calibrated with a Si reference cell certificated by NREL. All the solar cells were masked during the J-V measurements to define an active area of about 0.09 cm^2.

■ ASSOCIATED CONTENT

Supporting Information

Synthesis details, TGA data and comparison of various HTMs are given. This information is available free of charge via the Internet at http://pubs.acs.org/photonics.

■ AUTHOR INFORMATION

Corresponding Author

*E-mail: hong.wang@kaust.edu.sa; tao.wu@kaust.edu,sa

⊥ These authors contributed equally to this work.

Notes

The authors declare no competing financial interest.

■ ACKNOWLEDGMENTS

1
2
3
4
5
6
7
8
9
10
11
12
13
14
15
16
17
18
19
20
21
22
23
24
25
26
27
28
29
30
31
32
33
34
35
36
37
38
39
40
41
42
43
44
45
46
47
48
49
50
51
52
53
54
55
56
57
58
59
60

■ **REFERENCES**

(1) Kojima, A.; Teshima, K.; Shirai, Y.; Miyasaka,T. Organometal halide perovskites as visible-light sensitizers for photovoltaic cells. *J. Am. Chem. Soc.* **2009**, 131, 6050-6051.

(2) Lee, M. M.; Teuscher, J.; Miyasaka, T.; Murakami, T. N.; Snaith, H. J. Efficient hybrid solar cells based on meso-superstructured organometal halide perovskites. *Science* **2012**, 338, 643-647.

(3) Burschka, J.; Pellet, N.; Moon, S.-J.; Humphry-Baker, R.; Gao, P.; Nazeeruddin, M. K.; Grätzel, M. Sequential deposition as a route to high-performance perovskite-sensitized solar cells. *Nature* **2013**, 499, 316-319.

(4) Zhou, H.; Chen, Q.; Li, G.; Luo, S.; Song, T.-B.; Duan, H.-S.; Hong, Z.; You, J.; Liu, Y.; Yang, Y. Interface engineering of highly efficient perovskite solar cells. *Science* **2014**, 345, 542-546.

(5) Kim,H.-S.;   Lee, C.-R.;   Im, J.-H.;   Lee, K.-B.;   Moehl, T.;   Marchioro, A.; Moon, S.-J.;   Humphry-Baker, R.; Yum, J.-H.; Moser, J. E.; Grätzel, M.; Park, N.-G. Lead iodide perovskite sensitized all-solid-state submicron thin film mesoscopic solar cell with efficiency exceeding 9%. *Scientific Reports* **2012**, 2, 591.

(6) Heo, J. H.; Im, S. H.; Noh, J. H.; Mandal, T. N.; Lim, C.-S.; Chang, J. A.; Lee, Y. H.; Kim, H.-j.; Sarkar, A.; Nazeeruddin, M. K.; Grätzel, M.; Seok, S. I. Efficient

20

inorganic-organic hybrid heterojunction solar cells containing perovskite compound and polymeric hole conductors. *Nat. Photonics* **2013**, 7, 486-491.

(7) Qin, P.; Paek, S.; Dar, M. I.; Pellet, N.; Ko, J.; Grätzel, M.; Nazeeruddin, M. K. Perovskite Solar Cells with 12.8% Efficiency by Using Conjugated Quinolizino Acridine Based Hole Transporting Material. *J. Am. Chem. Soc.* **2014**, 136, 8516-8519.

(8) Liu, J.; Wu, Y.; Qin, C.; Yang, X.; Yasuda, T.; Islam, A.; Zhang, K.; Peng, W.; Chen, W.; Han, L. A dopant-free hole-transporting material for efficient and stable perovskite solar cells. *Energy Environ. Sci.* **2014**, 7, 2963-2967.

(9) Choi, H.; Park, S.; Paek, S.; Ekanayake, P.; Nazeeruddin, M. K.; Ko, J. Efficient star-shaped hole transporting materials with diphenylethenyl side arms for an efficient perovskite solar cell. *J. Mater. Chem. A.* **2014**, 19136-19140.

(10) Krishna, A.; Sabba, D.; Li, H.; Yin, J.; Boix, P. P.; Soci, C.; Mhaisalkar, S. G.; Grimsdale, A. C. Novel hole transporting materials based on triptycene core for high efficiency mesoscopic perovskite solar cells. *Chem. Sci.* **2014**, 5, 2702-2709.

(11) Li, H.; Fu, K.; Hagfeldt, A.; Grätzel, M.; Mhaisalkar, S. G.; Grimsdale, A. C. A Simple 3,4-Ethylenedioxythiophene Based Hole-Transporting Material for Perovskite Solar Cells. *Angew. Chem. Int. Ed.* **2014**, 53, 4085-4088.

(12) Xu, B.; Tian, H.; Bi, D.; Gabrielsson, E.; Johansson, E. M.; Boschloo, J. G.; Hagfeldt, A.; Sun, L. Efficient solid state dye-sensitized solar cells based on anoligomer hole transport material and an organic dye. *J. Mater. Chem. A.* **2013**, 1, 14467-14470.

(13) Christians, J. A.; Fung, R. C. M.; Kamat, P. V. An Inorganic Hole Conductor for Organo-Lead Halide Perovskite Solar Cells. Improved Hole Conductivity with Copper Iodide. *J. Am. Chem. Soc.* **2014**,136, 758-764.

(14) Chavhan, S.; Miguel, O.; Grande, H.-J.; Gonzalez-Pedro, V.; Sánchez, R. S.; Barea, E. M.; Mora-Seró, I.; Tena-Zaera, R. Organo-metal halide perovskite-based solar cells with CuSCN as inorganic hole selective contact. *J. Mater. Chem. A* **2014**, 2,12754-12760.

(15) Qin, P.; Tanaka, S.; Ito, S.; Tetreault, N.; Manabe, K.; Nishino, H.; Nazeeruddin, M. K.; Grätzel, M. Inorganic hole conductor-based lead halide perovskite solar cells with 12.4% conversion efficiency. *Nat. Commun.* **2014**, 5, 3834-3849.

(16) Xu, B.; Sheibani, E.; Liu, P.; Zhang, J.; Tian, H.; Vlachopoulos, N.; Boschloo, G.; Kloo, L.; Hagfeldt, A.; Sun, L. Carbazole‐Based Hole‐Transport Materials for Efficient Solid State Dye-Sensitized Solar Cells and Perovskite Solar Cells. *Adv. Mater.* **2014**, 26, 6629-6634.

(17) Lin, Y.; Li Y.; Zhan, X. Small molecule semiconductors for high efficiency organic photovoltaics. *Chem. Soc. Rev.* **2012**, 41, 4245-4272.

(18) Blouin, N.; Michaud, A.; Gendron, D.; Wakim, S.; Blair, E.; Neagu-Plesu, R.; Belletête, M.;   Durocher, G.; Tao, Y.; Leclerc, M. Toward a rational design of poly (2, 7-carbazole) derivatives for solar cells. *J. Am. Chem. Soc.* **2008**, 130, 732-742.

(19) Wang, Z.-S.; Koumura, N.; Cui, Y.; Takahashi, M.; Sekiguchi, H.; Mori, A.; Kubo, T.; Furube, A.; Hara, K. Hexylthiophene-functionalized carbazole dyes for

22

efficient molecular photovoltaics: tuning of solar-cell performance by structural modification. *Chem. Mater.* **2008**, 20, 3993-4003.

(20) Feng, Q.; Zhou, G.; Wang, Z.-S. Varied alkyl chain functionalized organic dyes for efficient dye-sensitized solar cells: Influence of alkyl substituent type on photovoltaic properties. *Journal of Power Sources* **2013**, 239, 16-23.

(21) Hagfeldt, A.; Boschloo, G.; Sun, L.; Kloo, L.; Pettersson, H. Dye sensitized solar cells. *Chem. Rev.* **2010**, 110, 6595-6663.

(22) Bach, U.; Lupo, D.; Comte, P.; Moser, J. E.; Weissörtel, F.; Salbeck, J.; Spreitzer, H.;Grätzel, M. Solid-state dye-sensitized mesoporous TiO2 solar cells with high photon-to electron conversion efficiencies. *Nature* **1998**, 395, 583-585.

(23) Kim, S. H.; Cho, I.; Sim, M. K.; Park, S.; Park, S. Y. Paek, Highly efficient deep-blue emitting organic light emitting diode based on the multifunctional fluorescent molecule comprising covalently bonded carbazole and anthracene moieties. *J. Mater. Chem.* **2011**, 21, 9139-9148.

(24) Leijtens, T.; Ding, I-K.; Giovenzana, T.; Bloking, Jason T.; McGehee, M. D.; Sellinger, A. Hole transport materials with low glass transition temperatures and high solubility for application in solid-state dye-sensitized solar cells, *ACS Nano* **2012**, 6, 1455-1462.

(25) Burschka, J.; Kessler, F.; Nazeeruddin, M. K.; Grätzel, M. Co (III) Complexes as p-Dopants in Solid-State Dye-Sensitized Solar Cells. *Chem. Mater.* **2013**, 25, 2986-2990.

23

(26) Koh, T. M.; Dharani, S.; Li, H.; Prabhakar, R. R.; Mathews, N.; Grimsdale, A. C.; Mhaisalkar, S. G. Cobalt Dopant with Deep Redox Potential for Organometal Halide Hybrid Solar Cells. *ChemSusChem* **2014**, 7, 1909-1914.

(27) Hagfeldt, A.; Boschloo, G.; Sun, L.; Kloo, L.; Pettersson, H. Dye-Sensitized Solar Cells. *Chem. Rev.* **2010**, 110, 6595-6663.

(28) Snaith, H. J.; Grätzel, M. Enhanced charge mobility in a molecular hole transporter via addition of redox inactive ionic dopant: Implication to dye-sensitized solar cells. *Appl. Phys. Lett.* **2006**, 89, 262114-262116.

(29) Stranks, S. D.; Eperon, G. E.; Grancini, G.; Menelaou, C.; Alcocer, M. J. P.; Leijtens, T.; Herz, L. M.; Petrozza, A.; Snaith, H. J. Electron-hole diffusion lengths exceeding 1 micrometer in an organometal trihalide perovskite absorber. *Science* **2013**, 342, 341-344.

(30) Mohammed, O. F.; Xiao, D.; Batista, V. S.; Nibbering, E. T. J. Excited-State Intramolecular Hydrogen Transfer (ESIHT) of 1,8-Dihydroxy-9,10-anthraquinone (DHAQ) Characterized by Ultrafast Electronic and Vibrational Spectroscopy and Computational Modeling. *J. Phys. Chem. A* **2014**, 118, 3090-3099.

24

1
2
3
4
5
6
7
8
9
10
11
12
13
14
15
16
17
18
19
20
21
22
23
24
25
26
27
28
29
30
31
32
33
34
35
36
37
38
39
40
41
42
43
44
45
46
47
48
49
50
51
52
53
54
55
56
57
58
59
60

For Table of Contents Use Only

Facile Synthesis and High performance of a New

Carbazole-Based Hole Transporting Material for Hybrid

Perovskite Solar Cells

Hong Wang* [a, ⊥], Arif D. Sheikh[a, ⊥], Quanyou Feng[b,c], Feng Li[a], Yin Chen[a], Weili Yu[a], Erkki Alarousu[d],

Chun Ma[a], Md Azimul Haque[a], Dong Shi[a], Zhong-Sheng Wang[b], Omar F. Mohammed [d], Osman M.

Bakr[a], Tom Wu*[a]

25